CHEST

Original Research

PULMONARY PROCEDURES

Toward the Guidance of Transbronchial Biopsy

Identifying Pulmonary Nodules With Optical Coherence Tomography

Lida P. Hariri, MD, PhD; Mari Mino-Kenudson, MD; Matthew B. Applegate, BS; Eugene J. Mark, MD; Guillermo J. Tearney, MD, PhD; Michael Lanuti, MD, FCCP; Colleen L. Channick, MD, FCCP; Alex Chee, MD; and Melissa J. Suter, PhD

Background: **Solitary pulmonary nodules (SPNs) frequently require transbronchial needle aspiration (TBNA) or biopsy to determine malignant potential, but have variable diagnostic yields. Confirming needle placement within SPNs during TBNA could significantly increase diagnostic yield. Optical coherence tomography (OCT) provides nondestructive, high-resolution, microstructural imaging with potential to distinguish SPN from parenchyma. We have developed needle-based OCT probes compatible with TBNA. Before OCT can play any significant role in guiding clinical TBNA, OCT interpretation criteria for differentiating SPN from lung parenchyma must be developed and validated.**

Methods: **OCT of SPN and parenchyma was performed on 111 ex vivo resection specimens. OCT criteria for parenchyma and SPN were developed and validated in a blinded assessment. Six blinded readers (two pulmonologists, two pathologists, and two OCT experts) were trained on imaging criteria in a 15-min training session prior to interpreting the validation data set.**

Results: **OCT of lung parenchyma displayed evenly spaced signal-void alveolar spaces, signal-intense backreflections at tissue-air interfaces, or both. SPNs lacked both of these imaging features. Independent validation of OCT criteria by the six blinded readers demonstrated sensitivity and specificity of 95.4% and 98.2%, respectively.**

Conclusions: **We have developed and validated OCT criteria for lung parenchyma and SPN with sensitivity and specificity $>95\%$ in this ex vivo study. We anticipate that OCT could be a useful complementary imaging modality to confirm needle placement during TBNA to potentially increase diagnostic yield.**

CHEST 2013; 144(4):1261–1268

Abbreviations: OCT = optical coherence tomography; SPN = solitary pulmonary nodule; TBNA = transbronchial needle aspiration; TB-OCT = transbronchial optical coherence tomography

Solitary pulmonary nodules (SPNs) detected by CT scan frequently require biopsy for tissue diagnosis. SPNs may be assessed via transthoracic fine-needle aspiration, which has high diagnostic yields but increased risk of pneumothorax.[1,2] Transbronchial needle aspiration (TBNA) may also be used to obtain tissue, with a lower risk of pneumothorax, but has variable diagnostic yield (14%-63%, depending on the size and location of the nodule).[1-4] The use of endobronchial ultrasound or electromagnetic navigation increases diagnostic yield, but the yields are still low, particularly for lesions ≤ 2.0 cm in diameter (33%-56%).[1-7] The addition of high-resolution imaging at the tip of the TBNA needle could further increase the diagnostic yield of endobronchial ultrasound or electromagnetic navigation-guided biopsy by confirming the needle placement within the target nodule prior to biopsy specimen acquisition.

Optical coherence tomography (OCT) is a nondestructive optical imaging modality that provides high-resolution, cross-sectional images of tissue microstructure at penetration depths approaching 2 to 3 mm.[8-14] The resolution (<10 μm) is comparable to low-power ($\times 4$), bright-field microscopy. These modalities have

been used with high accuracy in a wide variety of clinical applications, including catheter-based cardiovascular[11,15-23] and GI[9,11,24-29] imaging.

Bronchoscopic OCT imaging has been evaluated in ex vivo and in vivo lung pathology[30-39] and is capable of visualizing the fine features of normal airway layering and alveolar attachments. OCT imaging can identify pathologic changes, including preinvasive and preneoplastic airway lesions.[35] An ex vivo study with precisely matched OCT and histology described initial OCT features for common pulmonary pathologies, including airway-based and peripheral lung lesions.[37]

Needle-based OCT catheters have been developed.[38-43] Needle-based devices require flexibility to be compatible with standard bronchoscopes and/or TBNA needles. The previously developed OCT catheters are not capable of imaging and acquiring tissue through the same needle. We have developed a novel, flexible, transbronchial OCT (TB-OCT) catheter that is compatible with standard bronchoscopic TBNA needles and is capable of imaging and acquiring tissue through the same needle.[44] We anticipate that when the TB-OCT catheter is used as a complement to existing technologies, it will result in an increased diagnostic yield by confirming needle placement in real time prior to tissue acquisition. However, before OCT can play any significant role in guiding clinical TBNA, OCT imaging criteria for lung parenchyma and SPN must be developed and validated. In this study, we developed and validated OCT interpretation criteria for parenchyma and SPN in an ex vivo, blinded assessment with six independent readers, including pulmonologists, pathologists, and OCT experts.

Manuscript received March 4, 2013; revision accepted May 28, 2013.
Affiliations: From the Departments of Pathology (Drs Hariri, Mino-Kenudson, Mark, and Tearney), Pulmonary and Critical Care Unit (Mr Applegate and Drs Channick, Chee, and Suter), Wellman Center for Photomedicine (Drs Hariri, Tearney, Chee, and Suter and Mr Applegate), and Department of Thoracic Surgery (Dr Lanuti), Massachusetts General Hospital; Harvard Medical School (Drs Hariri, Mino-Kenudson, Mark, Tearney, Lanuti, Channick, and Suter); and Harvard-MIT Division of Health Sciences and Technology (Dr Tearney), Boston, MA.
Funding/Support: This work was funded in part by the National Institutes of Heath [Grants R00CA134920, R01CA167827, P41EB01593] and the American Lung Association [Grant RG-194681-N].
Correspondence to: Melissa J. Suter, PhD, Massachusetts General Hospital, 55 Fruit St, Warren Bldg, Room 407, Boston, MA 02114; e-mail: msuter@partners.org

DOI: 10.1378/chest.13-0534

Materials and Methods

Ex Vivo Image Criteria Development and Validation

Specimens: Fresh lung samples (111 tissue samples: 56 lung parenchyma and 55 SPN samples) from 48 ex vivo surgical and autopsy specimens were imaged with OCT. The Partners Human Research Committee Institutional Review Board approved this study (protocol number: 2010-P-002214/1).

Imaging System for Ex Vivo Imaging: The technical details of OCT have been described previously.[11,12] Briefly, the OCT system consists of a broadband wavelength-swept laser source (1,250-1,350 nm) at an A-line rate of 40 kHz. The axial resolution was 6 μm in tissue.[11,12] OCT images were obtained at 10 to 50 frames per second with either a custom-built, 2.4 to 5.1 F (0.8-1.7 mm diameter), helical scanning catheter or a dual-axis, benchtop scanner. Lung specimens were inflated during imaging with room air to 20 cm H_2O when possible. In the inflated lung specimens, images were collected transpleurally with the OCT catheter passed through a 15-gauge needle. In the samples imaged with needle-based OCT, needle localization within a lung nodule was confirmed via gross assessment and collection of tissues surrounding the needle subsequent to imaging. After imaging, tissues were fixed in formalin and submitted for histology for all specimens.

OCT Criteria Development and Training: A single SPN image and an uninflated lung parenchyma image were selected to develop OCT image interpretation criteria. Six blinded readers (two pathologists, two pulmonologists, and two OCT experts) were trained on the imaging criteria with these two selected images in a 15-min formal training session. The training images are displayed in Figure 1 and appear as they did in the training session.

Pathologic Interpretation of OCT Validation Data: Of the total 111 OCT images included in the study, two were used as training images. The training images were excluded from the validation set, which consisted of the remaining 109 images. The readers were blinded, and they independently reviewed the validation cases off-line. Readers were allowed to refresh themselves on the training images prior to interpretation of the validation set, but were not allowed access to the training images while interpreting the validation data set. Readers were instructed to record a single diagnosis of either SPN or lung parenchyma for each image. The length of time to complete interpretation was recorded for each reader and included both the time to interpret and record answers for all images. Histologic diagnoses of lung parenchyma or SPN were evaluated by an independent pathologist.

Statistics

The accuracy, sensitivity, and specificity of OCT criteria for differentiating SPNs from lung parenchyma were calculated by comparison with corresponding histologic diagnosis. The OCT interobserver variability among blinded OCT readers was quantified by the Cohen κappa test of concordance. All continuous variables are expressed as mean ± SD.

Results

OCT Criteria Development for SPN and Lung Parenchyma

Table 1 summarizes the OCT interpretation criteria for lung parenchyma and SPN. The OCT interpretation criteria for lung parenchyma included the

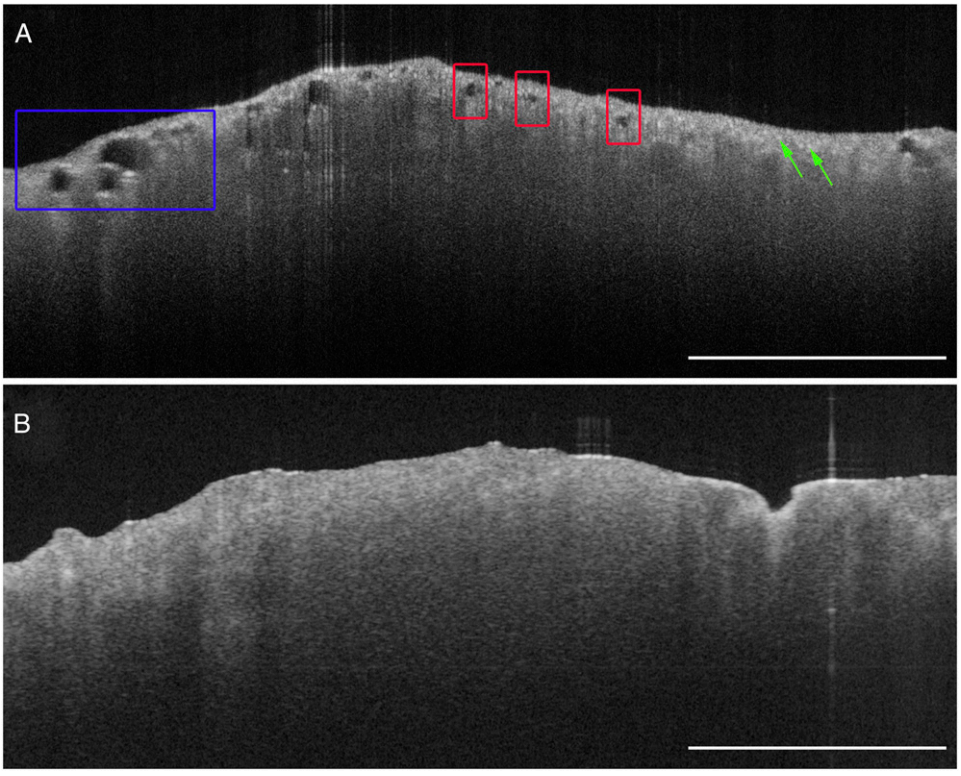

FIGURE 1. Training images. Ex vivo optical coherence tomography (OCT) images of uninflated lung parenchyma and solitary pulmonary nodule (SPN). A, OCT image of uninflated lung parenchyma obtained with a benchtop OCT system. The OCT imaging features of lung parenchyma are present, such as evenly spaced, signal-void alveolar spaces (regions in red boxes), some of which are larger in diameter when emphysematous change is present (region in blue box). Evenly spaced, signal-intense backreflections can be seen both in inflated and uninflated alveoli (green arrows). B, OCT image of a lung nodule obtained with a benchtop OCT system. OCT interpretation criteria for SPNs include the lack of both evenly spaced, signal-void alveolar spaces and signal-intense backreflections. Scale bars: 2 mm.

presence of evenly spaced, signal-void alveolar spaces and/or evenly spaced, high signal-intensity backreflections at tissue-air interfaces (Figs 1A, 2A, 2E). Atelectatic lung parenchyma was characterized by evenly spaced, high signal-intensity backreflections from collapsed alveolar walls but had a paucity of signal-void alveolar spaces (Fig 1A).

The OCT interpretation criteria for SPNs were the lack of both evenly spaced, signal-void alveoli and evenly spaced, high signal-intensity backreflections seen in lung parenchyma (Fig 1B). Typically, SPNs displayed a more homogenous appearance than lung parenchyma; however, fine-scale heterogeneities were present within nodules, the presence and characteristics of which varied based on the underlying pathology.[37]

Table 1—*OCT Interpretation Criteria for Lung Parenchyma and SPN*

Tissue Type	OCT Interpretation Criteria
Lung parenchyma	1. Signal-void alveolar spaces and/or 2. Evenly spaced, high signal-intensity backreflections
SPN	Lack of 1 and 2

OCT = optical coherence tomography; SPN = solitary pulmonary nodule.

In the needle-based OCT images of ex vivo human lung parenchyma (Fig 2), the alveoli display both of the OCT interpretation criteria for lung parenchyma. These alveoli have a larger diameter than seen in normal lung parenchyma due to emphysematous changes (Figs 2A, 2B, 2E).

A transition from SPN (adenocarcinoma) to lung parenchyma is demonstrated in Figure 2C. The ex vivo, needle-based OCT images of SPN lack both signal-void alveoli and signal-intense backreflections from tissue-air interfaces (Fig 2C, left side; Fig 2F). On the right-hand side of the longitudinal image (Fig 2C), there is a transition to hemorrhagic parenchyma, where signal-void alveoli are visualized with signal-intense backreflections from the tissue-air interfaces. The location of the transition from SPN to lung parenchyma was confirmed with histology (Fig 2D).

Blinded OCT Criteria Validation for SPNs and Lung Parenchyma

The clinical and specimen information for the ex vivo validation data set are summarized in Table 2. The 55 lung parenchyma cases were obtained from 17 lung

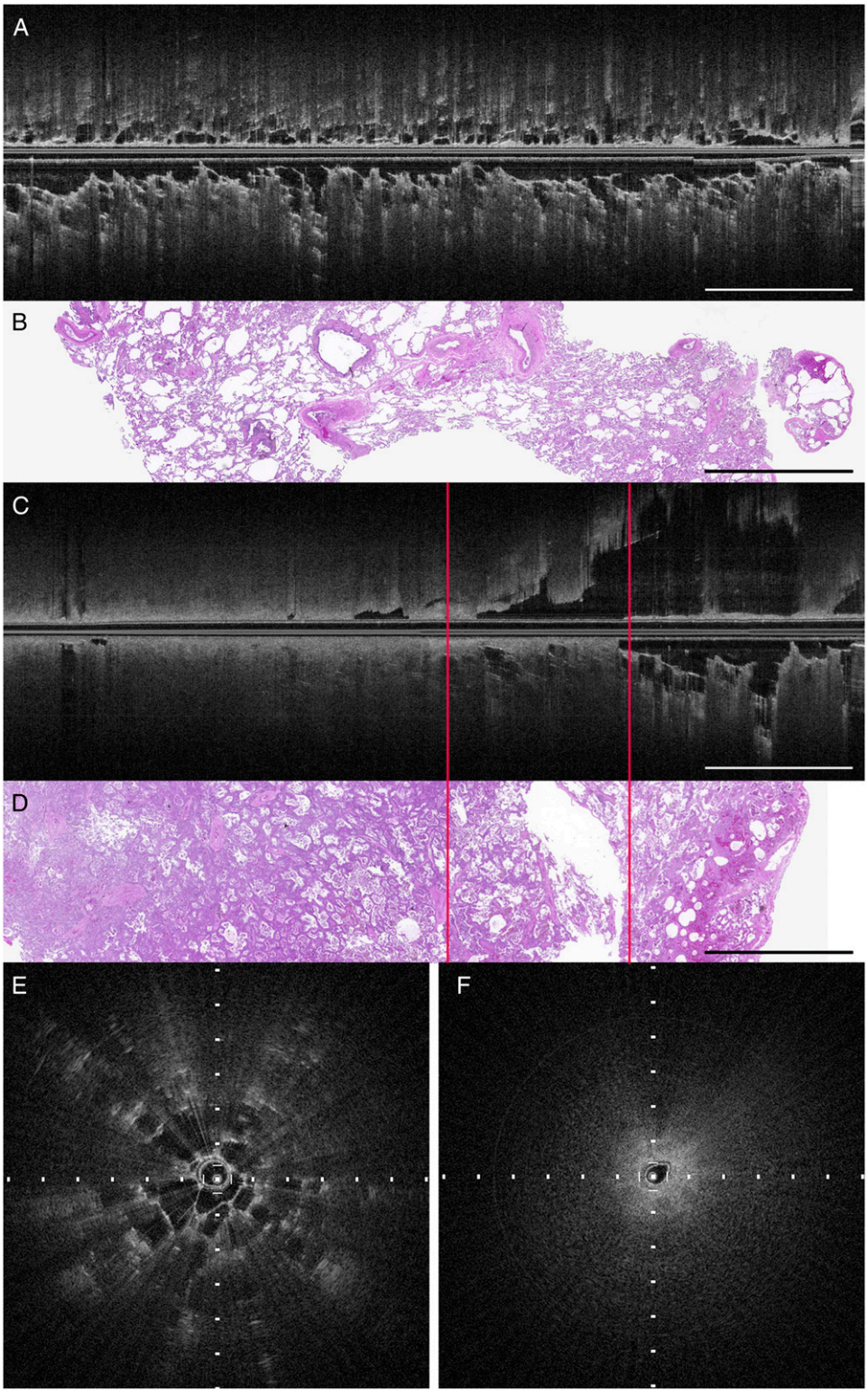

FIGURE 2. Ex vivo, transpleural, needle-based OCT image of inflated lung parenchyma and SPN. A, OCT longitudinal image of lung parenchyma away from pulmonary nodule, longitudinal section. B, Corresponding histology of lung parenchyma (hematoxylin and eosin). C, OCT longitudinal image of transition between SPN (adenocarcinoma, left of left line) and hemorrhagic parenchyma (right of right line). D, Corresponding histology demonstrating the transition between SPN (adenocarcinoma, left of left line) and hemorrhagic parenchyma (right of right line) (hematoxylin and eosin). Scale bars: 4 mm. E, Cross-sectional OCT image of lung parenchyma. F, Cross-sectional OCT image of pulmonary nodule (tick marks: 500 μm). See Figure 1 legend for expansion of abbreviations.

Table 2—*Summary of Clinical Data and Specimens Included in the Validation Data Set*

SPNs
54 specimens
24 primary adenocarcinomas
10 primary squamous cell carcinomas
4 pleomorphic carcinomas
3 adenosquamous carcinomas
3 mucoepidermoid carcinomas
3 hamartomas
1 carcinoid tumor
1 large cell neuroendocrine tumor
5 metastases
2 renal cell carcinomas
1 malignant peripheral nerve-sheath tumor
1 osteosarcoma
1 squamous cell carcinoma from the thyroid
Tumor size distribution
Mean: 2.8 cm
Median: 2.2 cm
Range: 1.0-9.5 cm
30 SPNs ≤ 3.0 cm
6 SPNs > 3.0 cm but ≤ 5.0 cm
3 SPNs > 5.0 cm

See Table 1 legend for expansion of abbreviation.

resection specimens and included 35 inflated lung parenchyma and 20 uninflated lung parenchyma specimens. Uninflated lung parenchyma specimens were included to simulate atelectasis, which may occasionally occur adjacent to an SPN in the in vivo setting. Parenchyma specimens with vascular congestion, hemorrhage, pneumonia, interstitial fibrosis, and emphysematous changes were also included in the validation data set. The 54 SPN OCT samples were obtained from 39 SPNs in 39 lung resection specimens and included a variety of benign and malignant lesions (Table 2). The SPNs averaged 2.8 cm in maximal dimension (range, 1.0-9.5 cm). A few specimens containing larger masses were included in this study to assess large peripheral masses that might be accessible by TBNA. In the larger diameter masses (n = 10), multiple, spatially discrete regions within each mass were imaged with OCT, particularly when the mass demonstrated gross heterogeneity.

Validation

The OCT interpretation criteria applied to the validation data set by the blinded OCT readers showed high sensitivity and specificity for distinguishing SPN from lung parenchyma (Table 3). The overall accuracy, sensitivity, and specificity of the six OCT readers were 96.8 ± 2.1%, 95.4 ± 5.1%, and 98.2 ± 2.3%, respectively. The interobserver variability among the blinded OCT readers was very low ($\kappa = 0.90$). The average time to interpret each image and record the diagnosis was approximately 14 s/image for the OCT experts (total: 26 min for 109 images) and 19 s/image for both the pulmonologists and pathologists (total: 35.3 min for 109 images).

Table 4 summarizes the false-positive and false-negative cases in the validation data set. There were four false-positive cases, which included three cases of uninflated lung parenchyma and one of inflated lung parenchyma. Of the false-positive uninflated parenchyma cases, one case was missed by two readers, whereas the other two cases were missed by one reader each. There were nine false-negative cases, which included five adenocarcinomas, one mucoepidermoid carcinoma, one hamartoma, one squamous cell carcinoma, and one metastatic osteosarcoma. In the false-negative adenocarcinoma cases, all the cases displayed small, atypical gland formation in the imaging field and two of the five cases also had blood contamination. Similarly, the mucoepidermoid carcinoma had many small glands. In all these cases, the glands were not evenly spaced and did not exhibit the signal-intense backreflections seen at tissue-air interfaces in lung parenchyma. The squamous cell carcinoma contained very small foci of entrapped alveolar parenchyma, creating focal regions in the OCT images with features of lung parenchyma. The hamartoma contained focal intranodular fat, which had imaging features similar to alveoli, such as signal-void spaces, but lacked the signal-intense backreflections seen at tissue-air interfaces in lung parenchyma. The metastatic osteosarcoma contained numerous irregularly shaped, thin-walled vessels, which mimicked alveolar-like spaces, but these also lacked the signal-intense backreflections seen at tissue-air interfaces in true alveoli (Table 4).

Discussion

In the National Lung Screening Trial, the false-positive rate for pulmonary nodules was 96.4% and 94.5% in the low-dose CT imaging group and the radiography group, respectively.[45] Because such a high percentage of these lesions are benign, SPNs must often undergo tissue biopsy for histologic diagnosis to determine malignant potential. TBNA is a low-risk

Table 3—*Validation of OCT Criteria for SPN and Lung Parenchyma*

Statistic	OCT Experts	Pathologists	Pulmonologists
Sensitivity	99.1 ± 1.3	93.5 ± 6.6	93.5 ± 6.6
Specificity	99.1 ± 1.3	98.2 ± 2.6	97.3 ± 3.9
Accuracy	99.1 ± 1.3	95.9 ± 1.95	95.4 ± 1.3
	All OCT Readers		
Sensitivity	95.4 ± 5.1	…	…
Specificity	98.2 ± 2.3	…	…
Accuracy	96.8 ± 2.1	…	…

Data given as mean %±SD. See Table 1 legend for expansion of abbreviations.

Table 4—*False-Negative and False-Positive Cases in the Validation Data Set*

Cases	No.	Likely Cause for Missed Interpretation	Features Possibly Improving Interpretation
False-positive cases	4		
Uninflated lung	3	Atelectasis mimicking mass	Identify evenly spaced, signal-intense backreflections
Inflated lung	1	Blood contamination	Identify evenly spaced, signal-intense backreflections
False-negative cases	9		
Adenocarcinoma	5	Small glands mimicking alveoli	Lack of even spacing and signal-intense backreflections
		Blood contamination	Lack of even spacing and signal-intense backreflections
Hamartoma	1	Fat within nodule mimicking alveoli	Lack of even spacing and signal-intense backreflections
Mucoepidermoid carcinoma	1	Small cystic spaces mimicking alveoli	Lack of even spacing and signal-intense backreflections
Squamous cell carcinoma	1	Very focal, entrapped alveoli within mass	Alveoli seen are focal, not diffuse
Metastatic osteosarcoma	1	Irregular vascular spaces mimicking alveoli	Lack of signal-intense backreflections

technique that can provide tissue for diagnosis, but it results in variable diagnostic yield (14%-63%) that is particularly low in nodules ≤ 2.0 cm in diameter.[1-4] OCT provides high-resolution, depth-resolved imaging with rapid acquisition rates and has the potential to assess needle placement in real time during TBNA. We have developed and described a TB-OCT catheter compatible with transbronchial imaging through a standard TBNA needle.[44] Before OCT imaging can play any significant role in guiding clinical TBNA, the ability of OCT to distinguish lung parenchyma and SPN must be assessed. In this study, we developed and validated OCT interpretation criteria for SPN and lung parenchyma ex vivo with high sensitivity and specificity (> 95%). These results support the ability of OCT to aid in the assessment of needle placement during TBNA of SPN, with potential to increase diagnostic yield.

The blinded readers achieved high sensitivity and specificity (> 95%) with rapid image-interpretation times after a short training with very few training images. Readers with little or no prior OCT experience had slightly lower sensitivity and specificity rates when compared with the near-perfect results of the OCT experts. It is expected that with additional experience and training, these readers will improve their ability to interpret images to more closely parallel the results of the OCT experts.

Specimens included in the blinded assessment encompassed a variety of pathologies, including benign hamartomas, peripheral carcinoids, and malignant primary and metastatic neoplasms. Nodules with hemorrhagic, necrotic, and fibrotic components were included to reproduce the diverse features encountered in SPNs in vivo. Similarly, lung parenchyma specimens with emphysematous change, hemorrhage, congestion, pneumonia, and interstitial fibrosis were also included. Given the high sensitivity and specificity, the inclusion of a variety of specimen types and quality, and the rapid image-interpretation speed of the blinded readers, it is anticipated that pulmonologists performing TBNA with OCT guidance would have little difficulty in assessing OCT images in real time to determine if the needle is properly targeted to the nodule.

Atelectasis can occur in the in vivo setting adjacent to a targeted mass, thus, the distinction of these entities is important. This study included both inflated and uninflated parenchyma specimens to simulate the features of parenchyma that may be encountered in vivo. The readers were able to differentiate both types of lung parenchyma from SPN with high sensitivity and specificity. However, nearly all the false-positive cases of lung parenchyma misclassified as nodule occurred in uninflated lung specimens (three of four false-positive cases). Atelectatic lung can mimic features of an SPN due to the paucity of signal-void alveolar spaces. However, evenly dispersed, signal-intense backreflections are present in uninflated lung and can indicate to the reader that the tissue consists of collapsed parenchyma rather than SPN.

All nine false-negative cases displayed signal-poor structures that mimicked the appearance of alveoli. However, these signal-poor structures were not evenly spaced and did not display the characteristic signal-intense backreflections seen at tissue-air interfaces in alveoli. It is anticipated that with increased experience, the readers will become even more apt at applying the OCT interpretation to determine whether a signal-void space is due to an alveolar space or a luminal structure within an SPN. Also, in the case of increased tumor vascularity, the addition of Doppler imaging to structural OCT could aid in distinguishing vessels from other structures.[46,47]

Imaging of ex vivo lung specimens as a surrogate to in vivo imaging presents some limitations. Motion artifacts may occur in the in vivo setting that are not reflected in ex vivo imaging. Successful in vivo OCT imaging of normal and diseased lung has previously been conducted and demonstrated images of comparable quality to ex vivo OCT images,[32-36] with minimal motion artifact. Thus, it is not anticipated that motion artifact will hinder image quality and/or interpretation. However, it is possible that respiratory motion may lead to issues with imaging and subsequent rebiopsy

of the same tissue sample due to gross movements of the needle within the target tissue. This will require further investigation in future in vivo studies.

Blood in the imaging field scatters and attenuates light. If blood contamination in vivo from procedural hemorrhage becomes a significant issue during imaging, small-volume saline flushes can be implemented to clear the field of view. This technique has been successfully implemented in intravascular imaging and should add no additional risk over a BAL. Additionally, the inclusion of Doppler imaging as a complementary modality to OCT imaging could identify vessels during in vivo imaging,[46,47] which may be subsequently avoided during tissue acquisition to decrease bleeding risks.

Surgical lung specimens containing a nodule often undergo pathologic frozen-section evaluation, during which the pleural surface and parenchyma are cut to assess the nodule, precluding specimen inflation. SPNs are frequently firm, and are not likely to have any significant change in OCT imaging features in the inflated vs uninflated state. However, the OCT criteria developed in this ex vivo study for parenchyma and SPN will need to be validated in the in vivo setting in future studies.

In this study, we developed and validated OCT interpretation criteria for SPN and lung parenchyma ex vivo, and achieved sensitivity and specificity of $>95\%$ with rapid image-interpretation times after a short training session. These results are encouraging for the use of OCT during TBNA for real-time needle placement assessments; however, these results will need to be further validated in vivo. Future clinical studies will aim to validate OCT criteria and assess TB-OCT-guided tissue yields in vivo. TB-OCT imaging has significant potential to increase diagnostic yield as a complementary imaging modality to assess needle placement in real time during TBNA.

Acknowledgments

Author contributions: Dr Suter had full access to all of the data in the study and takes responsibility for the integrity of the data and the accuracy of the data analysis.
Dr Hariri: contributed to the study design; collection, analysis, and interpretation of data; drafting and critical review of the manuscript; reading and approving the final version; and served as principal author.
Dr Mino-Kenudson: contributed to the collection, analysis, and interpretation of data; critical review of the manuscript; and reading and approving the final version.
Mr Applegate: contributed to the collection and analysis of data, critical review of the manuscript, and reading and approving the final version.
Dr Mark: contributed to the collection, analysis, and interpretation of data; critical review of the manuscript; and reading and approving the final version.
Dr Tearney: contributed to the development of the imaging system, analysis and interpretation of data, critical review of the manuscript, and reading and approving the final version.
Dr Lanuti: contributed to the analysis and interpretation of data, critical review of the manuscript, and reading and approving the final version.
Dr Channick: contributed to the analysis and interpretation of data, critical review of the manuscript, and reading and approving the final version.
Dr Chee: contributed to the collection of data, drafting and critical review of the manuscript, and reading and approving the final version.
Dr Suter: contributed to the study design; development of the imaging system and catheters; collection, analysis, and interpretation of data; drafting and critical review of the manuscript; and reading and approving the final version.
Financial/nonfinancial disclosures: The authors have reported to *CHEST* the following conflicts of interest: Dr Tearney receives consulting income from NinePoint Medical Inc, which has a licensing arrangement with Massachusetts General Hospital. Dr Suter receives clinical research support from NinePoint Medical Inc. Drs Tearney and Suter have the right to receive royalty payments from NinePoint Medical Inc. The remaining authors have reported to *CHEST* that no potential conflicts of interest exist with any companies/organizations whose products or services may be discussed in this article.
Role of sponsor: The sponsors had no role in the study design, execution, or analysis.
Other contributions: The authors would like to thank Stephen Conley; Sven Holder, BS; and the Wellman Center for Photomedicine Photopathology core for their contributions to this work.

References

1. Gould MK, Fletcher J, Iannettoni MD, et al. Evaluation of patients with pulmonary nodules: when is it lung cancer? ACCP evidence-based clinical practice guidelines (2nd ed). *Chest* 2007;132(suppl 3):108S-130S
2. Wang Memoli JS, Nietert PJ, Silvestri GA. Meta-analysis of guided bronchoscopy for the evaluation of the pulmonary nodule. *Chest*. 2012;142(2):385-393.
3. Baaklini WA, Reinoso MA, Gorin AB, Sharafkaneh A, Manian P. Diagnostic yield of fiberoptic bronchoscopy in evaluating solitary pulmonary nodules. *Chest*. 2000;117(4):1049-1054.
4. Rivera MP, Mehta AC. Initial diagnosis of lung cancer: ACCP evidence-based clinical practice guidelines (2nd edition). *Chest* 2007;132(suppl 3):131S-148S
5. Mazzone P, Jain P, Arroliga AC, Matthay RA. Bronchoscopy and needle biopsy techniques for diagnosis and staging of lung cancer. *Clin Chest Med*. 2002;23(1):137-158.
6. Shure D, Fedullo PF. Transbronchial needle aspiration of peripheral masses. *Am Rev Respir Dis*. 1983;128(6):1090-1092.
7. Steinfort DP, Khor YH, Manser RL, et al. Radial probe endobronchial ultrasound for the diagnosis of peripheral lung cancer: systematic review and meta-analysis. *Eur Respir J*. 2011;37(4):902-910.
8. Huang D, Swanson EA, Lin CP, et al. Optical coherence tomography. *Science*. 1991;254(5035):1178-1181.
9. Bouma BE, Tearney GJ, Compton CC, Nishioka NS. High-resolution imaging of the human esophagus and stomach in vivo using optical coherence tomography. *Gastrointest Endosc*. 2000;51(4 pt 1):467-474.
10. Yun S, Tearney G, de Boer J, Iftimia N, Bouma B. High-speed optical frequency-domain imaging. *Opt Express*. 2003;11(22):2953-2963.
11. Yun SH, Tearney GJ, Vakoc BJ, et al. Comprehensive volumetric optical microscopy in vivo. *Nat Med*. 2006;12(12):1429-1433.
12. Yun S, Tearney G, Bouma B, Park B, de Boer J. High-speed spectral-domain optical coherence tomography at 1.3 mum wavelength. *Opt Express*. 2003;11(26):3598-3604.
13. Yun S, Tearney G, de Boer J, Bouma B. Removing the depth-degeneracy in optical frequency domain imaging with frequency shifting. *Opt Express*. 2004;12(20):4822-4828.

14. Choma M, Sarunic M, Yang C, Izatt J. Sensitivity advantage of swept source and Fourier domain optical coherence tomography. *Opt Express*. 2003;11(18):2183-2189.
15. Brezinski ME, Tearney GJ, Bouma BE, et al. Optical coherence tomography for optical biopsy. Properties and demonstration of vascular pathology. *Circulation*. 1996;93(6):1206-1213.
16. Tearney GJ, Waxman S, Shishkov M, et al. Three-dimensional coronary artery microscopy by intracoronary optical frequency domain imaging. *JACC Cardiovasc Imaging*. 2008;1(6): 752-761.
17. Fujimoto JG, Boppart SA, Tearney GJ, Bouma BE, Pitris C, Brezinski ME. High resolution in vivo intra-arterial imaging with optical coherence tomography. *Heart*. 1999;82(2):128-133.
18. Bezerra HG, Costa MA, Guagliumi G, Rollins AM, Simon DI. Intracoronary optical coherence tomography: a comprehensive review clinical and research applications. *JACC Cardiovasc Interv*. 2009;2(11):1035-1046.
19. Farooq V, Serruys PW, Heo JH, et al. New insights into the coronary artery bifurcation hypothesis-generating concepts utilizing 3-dimensional optical frequency domain imaging. *JACC Cardiovasc Interv*. 2011;4(8):921-931.
20. Gogas BD, Farooq V, Onuma Y, et al. 3-dimensional optical frequency domain imaging for the evaluation of primary percutaneous coronary intervention in ST-segment elevation myocardial infarction. *Int J Cardiol*. 2011;151(1):103-105.
21. Kubo T, Xu C, Wang Z, van Ditzhuijzen NS, Bezerra HG. Plaque and thrombus evaluation by optical coherence tomography. *Int J Cardiovasc Imaging*. 2011;27(2):289-298.
22. Prati F, Jenkins MW, Di Giorgio A, Rollins AM. Intracoronary optical coherence tomography, basic theory and image acquisition techniques. *Int J Cardiovasc Imaging*. 2011;27(2): 251-258.
23. Prati F, Regar E, Mintz GS, et al; Expert's OCT Review Document. Expert review document on methodology, terminology, and clinical applications of optical coherence tomography: physical principles, methodology of image acquisition, and clinical application for assessment of coronary arteries and atherosclerosis. *Eur Heart J*. 2010;31(4):401-415.
24. Tearney GJ, Brezinski ME, Bouma BE, et al. In vivo endoscopic optical biopsy with optical coherence tomography. *Science*. 1997;276(5321):2037-2039.
25. Suter MJ, Vakoc BJ, Yachimski PS, et al. Comprehensive microscopy of the esophagus in human patients with optical frequency domain imaging. *Gastrointest Endosc*. 2008;68(4): 745-753.
26. Aguirre AD, Chen Y, Bryan B, et al. Cellular resolution ex vivo imaging of gastrointestinal tissues with optical coherence microscopy. *J Biomed Opt*. 2010;15(1):016025.
27. Chen Y, Aguirre AD, Hsiung PL, et al. Ultrahigh resolution optical coherence tomography of Barrett's esophagus: preliminary descriptive clinical study correlating images with histology. *Endoscopy*. 2007;39(7):599-605.
28. Qi X, Pan Y, Sivak MV, Willis JE, Isenberg G, Rollins AM. Image analysis for classification of dysplasia in Barrett's esophagus using endoscopic optical coherence tomography. *Biomed Opt Express*. 2010;1(3):825-847.
29. Testoni PA, Mangiavillano B. Optical coherence tomography in detection of dysplasia and cancer of the gastrointestinal tract and bilio-pancreatic ductal system. *World J Gastroenterol*. 2008;14(42):6444-6452.
30. Yang Y, Whiteman S, Gey van Pittius D, He Y, Wang RK, Spiteri MA. Use of optical coherence tomography in delineating airways microstructure: comparison of OCT images to histopathological sections. *Phys Med Biol*. 2004;49(7): 1247-1255.
31. Hanna N, Saltzman D, Mukai D, et al. Two-dimensional and 3-dimensional optical coherence tomographic imaging of the airway, lung, and pleura. *J Thorac Cardiovasc Surg*. 2005;129(3):615-622.
32. Su J, Zhang J, Yu L, G Colt H, Brenner M, Chen Z. Real-time swept source optical coherence tomography imaging of the human airway using a microelectromechanical system endoscope and digital signal processor. *J Biomed Opt*. 2008;13(3): 030506.
33. Suter MJ, Riker DR, Gallagher KA, et al. Real-time comprehensive microscopy of the pulmonary airways: a pilot clinical study. Poster presented at: American Thoracic Society 2009 International Conference; May 15-20, 2009; San Diego, CA.
34. Tsuboi M, Hayashi A, Ikeda N, et al. Optical coherence tomography in the diagnosis of bronchial lesions. *Lung Cancer*. 2005;49(3):387-394.
35. Lam S, Standish B, Baldwin C, et al. In vivo optical coherence tomography imaging of preinvasive bronchial lesions. *Clin Cancer Res*. 2008;14(7):2006-2011.
36. Michel RG, Kinasewitz GT, Fung KM, Keddissi JI. Optical coherence tomography as an adjunct to flexible bronchoscopy in the diagnosis of lung cancer: a pilot study. *Chest*. 2010;138(4):984-988.
37. Hariri LP, Applegate MB, Mino-Kenudson M, et al. Volumetric optical frequency domain imaging of pulmonary pathology with precise correlation to histopathology. *Chest*. 2013;143(1):64-74.
38. Lorenser D, Yang X, Kirk RW, Quirk BC, McLaughlin RA, Sampson DD. Ultrathin side-viewing needle probe for optical coherence tomography. *Opt Lett*. 2011;36(19):3894-3896.
39. Quirk BC, McLaughlin RA, Curatolo A, Kirk RW, Noble PB, Sampson DD. In situ imaging of lung alveoli with an optical coherence tomography needle probe. *J Biomed Opt*. 2011; 16(3):036009.
40. Kuo WC, Kim J, Shemonski ND, Chaney EJ, Spillman DR Jr, Boppart SA. Real-time three-dimensional optical coherence tomography image-guided core-needle biopsy system. *Biomed Opt Express*. 2012;3(6):1149-1161.
41. Yang VX, Mao YX, Munce N, et al. Interstitial Doppler optical coherence tomography. *Opt Lett*. 2005;30(14):1791-1793.
42. Zysk AM, Marks DL, Liu DY, Boppart SA. Needle-based reflection refractometry of scattering samples using coherence-gated detection. *Opt Express*. 2007;15(8):4787-4794.
43. Wu Y, Xi J, Huo L, et al. Robust high-resolution fine OCT needle for side-viewing interstitial tissue imaging. *IEEE Journal of Selected Topics in Quantum Electronics*. 2010;16(4): 863-869.
44. Tan KM, Shishkov M, Chee A, Applegate MB, Bouma BE, Suter MJ. Flexible transbronchial optical frequency domain imaging smart needle for biopsy guidance. *Biomed Opt Express*. 2012;3(8):1947-1954.
45. Aberle DR, Adams AM, Berg CD, et al; National Lung Screening Trial Research Team. Reduced lung-cancer mortality with low-dose computed tomographic screening. *N Engl J Med*. 2011;365(5):395-409.
46. Cense B, Chen TC, Nassif N, et al. Ultra-high speed and ultra-high resolution spectral-domain optical coherence tomography and optical Doppler tomography in ophthalmology. *Bull Soc Belge Ophtalmol*. 2006; (302):123-132.
47. Yang VX, Tang SJ, Gordon ML, et al. Endoscopic Doppler optical coherence tomography in the human GI tract: initial experience. *Gastrointest Endosc*. 2005;61(7):879-890.